

We are IntechOpen, the world's leading publisher of Open Access books Built by scientists, for scientists

4,900

Open access books available

124,000

International authors and editors

140M

Downloads

Our authors are among the

154

Countries delivered to

TOP 1%

most cited scientists

12.2%

Contributors from top 500 universities



WEB OF SCIENCE™

Selection of our books indexed in the Book Citation Index
in Web of Science™ Core Collection (BKCI)

Interested in publishing with us?
Contact book.department@intechopen.com

Numbers displayed above are based on latest data collected.
For more information visit www.intechopen.com



Subspace Techniques for Brain Signal Enhancement

Nidal S. Kamel and Mohd Zuki-Yusoff
*Universiti Teknologi Petronas
Malaysia*

1. Introduction

Human bodies can be considered as electrical generators that produce various biomedical signals. Examples of the biomedical signals that can be generated by the brain are evoked potentials, which include visual evoked potentials (VEPs), brainstem auditory evoked potentials (BAEPs), and somatosensory evoked potentials (SSEPs). In clinical environments, these potentials are used by clinicians as *signatures* to check the nerve signals (vision-, hearing-, or feel-triggered) that are transmitted to the brain and spinal cord.

Extracting the evoked potentials (EPs) from the brain is generally very difficult. The problem is caused by the presence of the spontaneous electroencephalograph (EEG) which contaminates heavily the desired signals. The ongoing EEG can be considered as colored noise since its frequency spectrum overlaps with that of the wanted signals. The EEG may degrade the overall signal-to-noise ratio (SNR) to as low as -10 dB (Regan, 1989; Henning, 1995).

The conventional method of “multi-trial” ensemble averaging (EA) does improve the SNR, but at the expense of longer recording time causing discomfort and fatigue to the subject under study. In fact, hundreds of response trials need to be gathered to obtain a satisfactorily clean estimate of EPs. Most importantly, EA introduces significant distortion and information loss since EPs are time varying (i.e., non-stationary) signals (Cui et al., 2004). In other words, since the waveform morphology (i.e., amplitude and shape) is not constant from one trial to another as experimented by (John et al., 1964), the averaging techniques tend to eliminate the trial-to-trial variations of the VEP signals which may prove useful to clinicians and other researchers.

For EP estimation, researchers have proposed various techniques utilizing different sorts of averaging and filtering which include Kalman filtering, Wiener filtering, wavelets, cumulants, etc. In this chapter, we discuss the subspace based EP extraction techniques and their potentials as single-trial estimators to replace the multi-trial based ones.

In subspace techniques for signal enhancement, the eigendecomposition of the covariance matrix of the noisy signal is used to decompose the matrix space into signal and noise subspaces. Retaining only the information in the signal subspace eigenvectors, that is, forming a lower-rank approximation of the covariance matrix effectively enhances the SNR because of the omission of the contribution of power in noise subspace. Many subspace techniques have been proposed over the last decade for EP extraction using the signal subspace, with different degrees of success. In this chapter, we outline the foundations of the proposed subspace techniques, through the aspects of bio-signal model development, creation and/or selection of the pertinent vector(s) and/or matrices, contaminated signal decorrelation and desired signal reconstruction processes. Three subspace techniques, especially designed for EP extraction, are discussed and compared in performance. The techniques are the generalized subspace approach (GSA) (Nidal-Kamel & Zuki-Yusoff, 2008), the subspace regularization method (SRM) (Karjalainen et al., 1999), and the subspace dynamical estimation method (SDEM) (Georgiadis et al., 2007). Furthermore, a criterion for defining the signal subspace dimension is suggested and analyzed.

The chapter is organized as follows. The fundamental concepts of subspace techniques are presented in section 2. The three subspace techniques namely GSA, SRM and SDEM are discussed in section 3. Section 4 describes the results in simulated and real environments and section 5 concludes the chapter.

For clarity, an attempt has been made to adhere to a standard notational convention. Lower case **boldface** characters will generally refer to vectors. Upper case **BOLDFACE** characters will generally refer to matrices. Vector or matrix transposition will be denoted using $(.)^T$ and $(.)^*$ denotes conjugation for complex valued signals. $\mathfrak{R}^{K \times K}$ denotes the real vector space of $K \times K$ dimensions.

2. Fundamental Concepts of Subspace Techniques

Consider $A \in \mathfrak{R}^{M \times M}$ as the autocorrelation matrix of the noisy EP signal. It has been found in many signal processing applications that the eigendecomposition of the matrix A can be used to decompose the matrix space into principal or signal subspace and noise subspace. This distinctive separation can be used to improve methods of signal enhancement and signal parameter estimation.

Principal component analysis, originating in work by Karl Pearson around the turn of the last century and further developed in 1930s by Harold Hotelling, consists of finding an orthogonal transformation of the original – stochastic- variables to a new set of uncorrelated variables, which are derived in non-increasing order of importance. These so-called principal components are linear combinations of the original variables such that their first few components will account for most of the variations in the original data, effectively reducing the dimensionality of the data (Deprettere, 1989). Since, the concept of oriented energy is closely related to principal components analysis, we start our work using this definition.

2.1 Oriented Energy

The column vectors of an $M \times M$ matrix A are considered to form an indexed set of M vectors, denoted by $\{a_k\}$, $k = 1, 2, \dots, M$. An M -dimensional vector q and the direction it represents in a vector space are used as synonyms.

Definition 1. Energy of a vector sequence.

Consider a sequence of M -vectors $\{a_k\}$, $k = 1, 2, \dots, M$ and associated real $M \times M$ matrix A . Its total energy $E[A]$ is defined via Frobenius norm of the $M \times M$ matrix A :

$$E(A) = \|A\|_F^2 = \sum_{i=1}^M \sum_{j=1}^M a_{ij}^2 \quad (1)$$

Definition 2. Oriented energy.

Let A be an $M \times M$ matrix and denote its M column vectors as a_k , $k = 1, 2, \dots, M$. For the indexed vector set $\{a_k\}$ of M -vectors $a_k \in \mathfrak{R}^M$ and for any unit vector $q \in \mathfrak{R}^M$, the energy E_q measured in direction q , is defined as:

$$E_q(A) = \sum_{k=1}^M (q^T \cdot a_k)^2 \quad (2)$$

More generally, the energy E_Q measured in a subspace $Q \subset \mathfrak{R}^M$, is defined as:

$$E_Q(A) = \sum_{k=1}^M \|P_Q(a_k)\|^2 \quad (3)$$

where $P_Q(a_k)$ denotes the orthogonal projection of a_k into the subspace Q and $\|\cdot\|$ denotes the Euclidean norm. In other words, the oriented energy of a vector sequence $\{a_k\}$, measured in the direction q (subspace Q) is the energy of the signal, projected orthogonally on to the vector q (subspace Q).

2.2 Oriented Energy and Eigendecomposition of $A \in \mathfrak{R}^{M \times M}$

In section 2.1, attention was given to the basic concepts of the oriented energy distribution. In this section, the tools which allow numerical characterization of the oriented energy concept will be studied.

The eigenvalue decomposition (ED) of matrix $A \in \mathfrak{R}^{M \times M}$, is a factorization process where a diagonalizable matrix is represented in terms of its eigenvectors and eigenvalues. The eigenvectors are represented by a non-singular matrix whose columns represent individual eigenvectors that are orthonormal to each other. The eigenvectors' corresponding eigenvalues are held and represented diagonally by a singular matrix.

Theorem 1. Let the columns v_1, v_2, \dots, v_M be the eigenvectors corresponding to the set of eigenvalues $\lambda_1, \lambda_2, \dots, \lambda_M$ of the square basis matrix $A \in \mathfrak{R}^{M \times M}$. Let $V \in \mathfrak{R}^{M \times M}$ be the matrix that holds the eigenvectors such that

$$V = [v_1 \ v_2 \ \dots \ v_M] \in \mathfrak{R}^{M \times M} \quad (4)$$

and Λ be the diagonal that holds the eigenvalue entries such that

$$\Lambda = \text{diag}[\lambda_1 \ \lambda_2 \ \dots \ \lambda_M] \quad (5)$$

in which, the eigenvalues have been ordered in decreasing values $\lambda_1 \geq \lambda_2 \geq \dots \lambda_M$. Then the matrix A will have a linearly independent set of M eigenvectors if and only if A can be expressed as

$$A = V\Lambda V^T \quad (6)$$

If the nonsingular matrix A also has Hermitian symmetry, then $V^{-1} = V^H$ and $\Lambda = \Lambda^H$. This means that a Hermitian matrix has real eigenvalues and that, if all the eigenvalues are distinct, the eigenvectors form an orthogonal set, because $VV^H = \sum v_i v_i^H = I$, that is, V is a unitary matrix. Thus the Hermitian matrix A which is diagonalized by a unitary transformation, will have the unique eigendecomposition (ED)

$$A = V\Lambda V^H \quad (7)$$

Proof. A proof of the ED theorem is given in (Golub & Van Loan, 1989).

Lemma 1: The number of non-zero eigenvalues is equal to the algebraic rank of the matrix A .

Lemma 2: Via the ED, the matrix A can be written as the sum of $r = \text{rank}(A)$ rank-one matrices; that is

$$A = \sum_{i=1}^r v_i \lambda_i v_i^{-1} \quad (8)$$

where $(v_i, \lambda_i, v_i^{-1})$ is the i^{th} eigen triplet of A .

Lemma 3: The Frobenius norm of $A \in \mathfrak{R}^{M \times M}$ of rank r is

$$\|A\|_F^2 = \sum_{i=1}^M \sum_{j=1}^M a_{ij}^2 = \sum_{k=1}^r \lambda_k \quad (9)$$

where λ_k are the eigenvalues of A .

The total energy in a vector sequence $\{a_k\}$ associated with matrix A , as stated in Definition 1, is equal to the energy in the eigenspectrum.

The smallest non-zero eigenvalue corresponds to the distance (in Frobenius norm) of the matrix to the closest matrix of lower rank. This property makes ED attractive tool in segregating the signal subspace from the noise subspace.

2.2.1 Conceptual relations between ED and oriented energy

We are now in the position to establish the link between the eigendecomposition and the concept of oriented energy distribution.

Define the unit ball UB in \mathfrak{R}^M as $UB = \{ \mathbf{q} \in \mathfrak{R}^M \mid \|\mathbf{q}\|_2 = 1 \}$.

Theorem 2. Consider a sequence of M -vectors $\{\mathbf{a}_k\}$, $k = 1, 2, \dots, M$ and the associated $M \times M$ matrix A with ED as defined in Eq. (6). Then,

$$E_{\mathbf{v}_i}(A) = \lambda_i \quad (10)$$

$\forall \mathbf{q} \in UB$: if $\mathbf{q} = \sum_{i=1}^M \gamma_i \cdot \mathbf{v}_i$, then

$$E_{\mathbf{q}}(A) = \sum_{i=1}^M \gamma_i \cdot \lambda_i \quad (11)$$

Proof. Trivial from Theorem 1.

Based on Theorem 2, the following observations can be made:

- The oriented energy measured in the direction of the i^{th} eigenvector of A is equal to the i^{th} eigenvalue.
- The energy in an arbitrary direction \mathbf{q} is the linear combination of the "orthogonal" oriented energies associated with the eigenvectors. If A is rank deficient, then there exists directions in \mathfrak{R}^M that contains no energy at all.

Furthermore, Theorem 2 can be used to obtain the directions and spaces of extremal energies.

Corollary 1: Under the assumptions of Theorem 2, the following properties follow:

Property 1 $\max_{\mathbf{q} \in UB} E_{\mathbf{q}}(A) = E_{\mathbf{v}_1}(A) = \lambda_1$

Property 2 $\min_{\mathbf{q} \in UB} E_{\mathbf{q}}(A) = E_{\mathbf{v}_M}(A) = \lambda_M$

Property 3 $\max_{Q^r \subset \mathfrak{R}^M} E_{Q^r}(A) = E_{S_V^r}(A) = \sum_{i=1}^r \lambda_i$

Property 4 $\min_{Q^r \subset \mathfrak{R}^M} E_{Q^r}(A) = E_{(S_V^{M-r})^\perp}(A) = \sum_{i=M-r+1}^M \lambda_i$

where "max" and "min" denote operators, respectively maximizing or minimizing the overall r -dimensional subspace Q^r of \mathfrak{R}^M ; S_V^r is the r -dimensional principal subspace of A ; and $(S_V^{M-r})^\perp$ represents the R -dimensional orthogonal complement of S_V^{M-r} .

Proof. Properties 1 through 4 follow immediately from the ED Theorems 1 and 2.

In words, Properties 1 and 2 relate the ED to the minima and maxima of the oriented energy distribution. The r -th principal subspace S_V^r is the one, among all r -dimensional subspaces of \mathfrak{R}^M , that senses a maximal oriented energy (Property 3). Properties 3 and 4 show that the orthogonal decomposition of the energy via the eigenvalue decomposition is canonical in the sense that it allows subspaces of dimension r to be found where the sequence has minimal and maximal energy. This decomposition of the ambient space, as the direct sum of a space of maximal and minimal energy for a given vector sequence, leads to very interesting rank consideration.

Now, if A ($M \times M$) represents the autocorrelation matrix of data corrupted by additive white noise, then it can be written as

$$A = S + N \quad (12)$$

in which S is the signal correlation matrix and N is the noise autocorrelation matrix, given in the case of white noise as

$$N = \sigma^2 I \quad (13)$$

where σ^2 is the noise variance.

The signal matrix will have the eigendecomposition

$$S = \sum_{i=1}^r \lambda_i \mathbf{v}_i \mathbf{v}_i^H \quad (14)$$

The eigenvectors $\mathbf{v}_1, \mathbf{v}_2, \dots, \mathbf{v}_r$, known as the principal subspace (as previously indicated), span the same signal subspace.

The noise matrix has the eigendecomposition

$$N = \sum_{i=r+1}^M \lambda_i \mathbf{v}_i \mathbf{v}_i^H = \sigma^2 \sum_{i=r+1}^M \mathbf{v}_i \mathbf{v}_i^H \quad (15)$$

Substitution of Eqs. (14) and (15) into Eq. (12) yields the eigendecomposition of the autocorrelation matrix

$$A = \sum_{i=1}^r \lambda_i \mathbf{v}_i \mathbf{v}_i^H + \sigma^2 \sum_{i=r+1}^M \mathbf{v}_i \mathbf{v}_i^H = \sum_{i=1}^r (\lambda_i + \sigma^2) \mathbf{v}_i \mathbf{v}_i^H + \sum_{i=r+1}^M \sigma^2 \mathbf{v}_i \mathbf{v}_i^H \quad (16)$$

Thus, the eigenvectors $\mathbf{v}_{r+1}, \mathbf{v}_{r+2}, \dots, \mathbf{v}_M$, span the noise subspace of A , all with the identical eigenvalue σ^2 . The principal eigenvectors $\mathbf{v}_1, \mathbf{v}_2, \dots, \mathbf{v}_r$ span the signal subspace of both A and S , with eigenvalues of $\lambda_1 + \sigma^2, \lambda_2 + \sigma^2, \dots, \lambda_r + \sigma^2$.

The eigendecomposition of the autocorrelation matrix in Eq. (16) can be exploited in the following way to generate improved signal estimators. Retaining only the information in the signal subspace eigenvectors, that is, forming a lower-rank approximation of A , effectively enhances the SNR because of the omission of the contribution of power in the noise subspace components. This is the basis of principal component (signal subspace) signal estimators.

Having established the link between the principal subspace (signal subspace) and the maximal energy of the signal, and between the noise subspace and the energy of the noise, we are in a position to show how this link is utilized by the different subspace techniques for EP enhancement.

3. The Subspace Techniques

3.1 The Generalized Subspace Approach

The generalized subspace approach (GSA) was proposed by (Nidal-Kamel & Zuki-Yusoff, 2008) as a subspace technique for EP signal enhancement in colored noise environment. This approach is an extension of (Ephraim & Van Trees, 1995) towards colored noise without the need for prewhitening. Other variations of subspace approaches to extract EPs can be found in (Zuki-Yusoff et al., 2009; Zuki-Yusoff et al., 2008; Zuki-Yusoff et al., 2007). The considered problem is to extract the clean EP signal $x(t)$ from the degraded EP signal by the brain background colored noise, $y(t)$. A K -dimensional vector of VEP samples \mathbf{y} is defined as follows:

$$\mathbf{y}(k) = \left[y\left(\frac{0}{f_s}\right), y\left(\frac{1}{f_s}\right), \dots, y\left(\frac{K-1}{f_s}\right) \right]^T \quad (17)$$

where f_s is the sampling frequency and $(.)^T$ denotes the transpose operation. Also, let \mathbf{y} denote the corresponding K -dimensional vector of the noisy EP. Since noise is assumed to be additive, we have

$$\mathbf{y}(k) = \mathbf{x}(k) + \mathbf{n}(k) \quad (18)$$

where \mathbf{x} is the K -dimensional vector of the original (clean) EP signal, and \mathbf{n} is the K -dimensional noise vector. Now, let \mathbf{H} be a $K \times K$ linear estimator of the clean EP vector as follows:

$$\hat{\mathbf{x}}(k) = \mathbf{H}(k) \bullet \mathbf{y}(k) \quad (19)$$

It is to be noted that the time index k shown in Eqs. (18) and (19) is for comprehensiveness and clarity. In the subsequent discussions, any vector or matrix that appears without a time index should be visualized as having k as its time index.

The error signal obtained in this estimation is given by

$$\begin{aligned}
\boldsymbol{\varepsilon} &= \hat{\boldsymbol{x}} - \boldsymbol{x} \\
&= \boldsymbol{H}\boldsymbol{y} - \boldsymbol{x} \\
&= (\boldsymbol{H} - \boldsymbol{I})\boldsymbol{x} + \boldsymbol{H}\boldsymbol{n} \\
&= \boldsymbol{\varepsilon}_x + \boldsymbol{\varepsilon}_n \quad \text{where } \boldsymbol{\varepsilon}_x = (\boldsymbol{H} - \boldsymbol{I})\boldsymbol{x} \quad \text{and } \boldsymbol{\varepsilon}_n = \boldsymbol{H}\boldsymbol{n}
\end{aligned} \tag{20}$$

where $\boldsymbol{\varepsilon}_x$ represents signal distortion and $\boldsymbol{\varepsilon}_n$ represents residual signal. Let

$$\begin{aligned}
\bar{\boldsymbol{\varepsilon}}_x^2 &= E\{\boldsymbol{\varepsilon}_x^T \boldsymbol{\varepsilon}_x\} = \text{tr}(E\{\boldsymbol{\varepsilon}_x \boldsymbol{\varepsilon}_x^T\}) \\
&= \text{tr}((\boldsymbol{H} - \boldsymbol{I})\boldsymbol{R}_x(\boldsymbol{H} - \boldsymbol{I})^T)
\end{aligned} \tag{21}$$

be the energy of the signal distortion vector. Similarly, let

$$\begin{aligned}
\bar{\boldsymbol{\varepsilon}}_n^2 &= E\{\boldsymbol{\varepsilon}_n^T \boldsymbol{\varepsilon}_n\} = \text{tr}(E\{\boldsymbol{\varepsilon}_n \boldsymbol{\varepsilon}_n^T\}) \\
&= \text{tr}(\boldsymbol{H}\boldsymbol{R}_n\boldsymbol{H}^T)
\end{aligned} \tag{22}$$

denote the energy of the residual noise, so that the total residual energies $\bar{\boldsymbol{\varepsilon}}^2$ become

$$\bar{\boldsymbol{\varepsilon}}^2 = \bar{\boldsymbol{\varepsilon}}_x^2 + \bar{\boldsymbol{\varepsilon}}_n^2 \tag{23}$$

The terms \boldsymbol{R}_x and \boldsymbol{R}_n in Eq. (21) and Eq. (22) refer to the covariance matrices of the clean signal and noise vectors, respectively. Since the EP and noise signals are independent as illustrated in Eq. (18), their covariance matrices also add linearly to produce the covariance matrix of the noisy EP \boldsymbol{R}_y ; that is,

$$\boldsymbol{R}_y = \boldsymbol{R}_x + \boldsymbol{R}_n \tag{24}$$

In practice, the covariance matrix of the noisy signal \boldsymbol{R}_y can be estimated directly from the observed (noisy) EP samples. Also, the noise covariance matrix \boldsymbol{R}_n can be computed using the pre-stimulation EEG samples during which the EP signals are absent. Indirectly, \boldsymbol{R}_x can be calculated by subtracting \boldsymbol{R}_n from \boldsymbol{R}_y . Now that \boldsymbol{R}_x and \boldsymbol{R}_n are known, the optimum linear estimator with time domain constraints on the residual noise is defined as follows (Ephraim & Van Trees, 1995):

$$\boldsymbol{H}_{opt} = \min_{\boldsymbol{H}} \bar{\boldsymbol{\varepsilon}}_x^2 \quad \text{subject to: } \bar{\boldsymbol{\varepsilon}}_n^2 \leq K\sigma^2 \tag{25}$$

where K is the dimension of the noisy vector space and σ^2 is a positive constant noise threshold level. The σ^2 in Eq. (25) dictates the amount of the residual noise allowed to remain in the linear estimator. Reducing noise in the given noisy EP signal causes some distortion in the extracted EP components. In the above optimization, by decreasing the noise threshold level σ^2 , we can decrease the amount of the residual noise and therefore, increase the amount of distortion and vice versa. Therefore, an acceptable value of σ^2 needs to be chosen so that the EP signal distortion is minimal and the EEG colored noise residue is not excessive. The optimal distortion in the sense of Eq. (25) can be found using *Kuhn-Tucker* necessary conditions for constrained minimization. Specifically, \boldsymbol{H} is a stationary feasible point and hence a minimizer, if it satisfies the gradient equation of the Lagrangian

$$L(\mathbf{H}, \mu) = \bar{\epsilon}_x^2 + \mu(\bar{\epsilon}_n^2 - K\sigma^2) \quad (26)$$

and

$$\mu(\bar{\epsilon}_n^2 - K\sigma^2) = 0 \quad \text{for } \mu \geq 0 \quad (27)$$

where μ is the Lagrangian multiplier. By setting the gradient equation $\nabla_{\mathbf{H}}L(\mathbf{H}, \mu) = 0$, we obtain

$$\begin{aligned} \frac{\partial L(\mathbf{H}, \mu)}{\partial \mathbf{H}} &= 0 \\ \Rightarrow \frac{\partial}{\partial \mathbf{H}} [\text{tr}((\mathbf{H} - \mathbf{I})\mathbf{R}_x(\mathbf{H} - \mathbf{I})^T)] + \frac{\partial}{\partial \mathbf{H}} [\mu \text{tr}(\mathbf{H}\mathbf{R}_n\mathbf{H}^T)] &= 0 \\ \Rightarrow (\mathbf{H} - \mathbf{I})\mathbf{R}_x + \mu\mathbf{H}\mathbf{R}_n &= 0 \\ \Rightarrow \mathbf{H}(\mathbf{R}_x + \mu\mathbf{R}_n) - \mathbf{R}_x &= 0 \end{aligned} \quad (28)$$

Subsequently, the gradient equation in Eq. (28) fulfilling Eq. (25) can be solved to yield the following estimator

$$\mathbf{H} = \mathbf{R}_x(\mathbf{R}_x + \mu\mathbf{R}_n)^{-1} \quad (29)$$

Next, the values for μ and σ^2 satisfying Eq. (27) need to be determined. Equation (27) can be simplified to yield

$$\bar{\epsilon}_n^2 = K\sigma^2 \quad (30)$$

The following expression for σ^2 is obtained by equating Eq. (30) with Eq. (22):

$$\begin{aligned} \bar{\epsilon}_n^2 = K\sigma^2 &= \text{tr}(\mathbf{H}\mathbf{R}_n\mathbf{H}^T) \\ \Rightarrow \sigma^2 &= \frac{1}{K} \text{tr}(\mathbf{H}\mathbf{R}_n\mathbf{H}^T) \end{aligned} \quad (31)$$

A meaningful relationship between σ^2 and μ is established by putting \mathbf{H} computed in Eq. (29) into Eq. (31).

$$\sigma^2 = \frac{1}{K} \text{tr}(\mathbf{R}_x^2(\mathbf{R}_x + \mu\mathbf{R}_n)^{-2}\mathbf{R}_n) \quad (32)$$

One issue that arises from Eq. (32) is whether to first specify the permissible level of residual noise σ^2 , or the Lagrange multiplier μ . The first approach is specify σ^2 in Eq. (32) and calculate μ from it. On the other hand, μ can be carefully chosen so that σ^2 can be calculated. Practically, the latter approach is normally used since μ can be computed without using Eq. (32) which is computationally expensive. Nonetheless, it is crucial to meet the necessary conditions stipulated in Eq. (32). From Eq. (32), we observe that $\sigma^2 \in [0, \sigma_{\max}^2]$ when $\mu \in [0, \infty]$, where $\sigma^2 = 0$ implies that $\mu = \infty$, and $\sigma^2 = \sigma_{\max}^2 = \frac{1}{K} \text{tr}(\mathbf{R}_n)$ yields $\mu = 0$.

Therefore, μ which satisfies Eq. (32) also satisfies Eq. (27). Hence, μ must also be the Lagrange multiplier for the time-domain-constrained (TDC) optimization problem of

Eq. (25). Further, there is a sufficient condition to be satisfied in order for H to be a minimizer; that is, the following second derivative must be positive definite.

$$L''(H, \mu) = \frac{\partial^2 L(H, \mu)}{\partial H^2} = R_x + \mu R_n \quad (33)$$

The noise covariance matrix R_n in Eq. (33) is always positive definite. However, it is not always the case for the signal covariance matrix R_x , which is initially derived by subtracting R_n from R_y . For a relatively high SNR, R_x is positive definite. As the SNR drops, R_x can be negative semidefinite. Nonetheless, μ is a positive number and R_n is still greater (for SNR < 0 dB) than R_x in any case, guaranteeing $L''(H, \mu)$ to be positive definite all the time and enabling H to be a minimizer.

It is clear that the filter matrix H derived in Eq. (29) is dependent on three parameters namely R_x , R_n and μ . Without further manipulation, H stated in Eq. (29) will function as a fixed filter; it will perform well to estimate the desired signal for a relatively high SNR value. As the SNR value degrades, it is desirable if H can be adjusted accordingly to minimize the noise residues while keeping the signal distortion at a minimal level.

One possible way to achieve an adjustable H is by taking the eigendecomposition of the R_x and R_n terms in Eq. (29). When the R_x and R_n are represented by their respective eigenvectors and eigenvalues, the fixed filter matrix H then becomes adjustable. If the dimension of the R_x eigenvalues is not lowered, the filter H functions exactly as that denoted in Eq. (29) — keeping signal distortion to its very minimum and noise energy to its maximum. However, when the dimension of R_x is lowered to a certain rank, the filter H will eliminate certain noise portions. If the proper dimension L of the R_x eigenvalues is chosen such that L spans only the signal subspace, the component in the “noise only” subspace will get nulled. The component that remains available at the output of the filter H is the wanted signal from the “signal” subspace. Of course, the wanted signal may not be completely free from noise since the “signal” subspace is actually a “signal plus noise” subspace. Nevertheless, the wanted signal is now clearly visible as the SNR value gets improved due to the subspace filtering technique.

For colored noise, an explicit prewhitening stage is normally required to prewhiten the corrupted data. For example, the covariance matrix R_x can be explicitly whitened by multiplying it with the $R_n^{-1/2}$ or R_n^{-1} term. Alternatively, the prewhitening process can be implicitly performed by means of the generalized eigendecomposition of R_x and R_n (Nidal-Kamel & Zuki-Yusoff, 2008). In other words, the eigendecomposition of a matrix can be generalized to a decomposition of the matrix pair (R_x, R_n) , as follows:

$$R_x V = R_n V \Lambda \quad (34)$$

where D diagonal $K \times K$ matrix that contains the generalized eigenvalues D and V contains the generalized non-unitary eigenvectors. The following relationships are also established from the generalized ED:

$$\mathbf{R}_x = \mathbf{V}^{-T} \mathbf{D} \mathbf{V}^{-1} \quad (35)$$

$$\mathbf{R}_n = \mathbf{V}^{-T} \mathbf{I} \mathbf{V}^{-1} \quad (36)$$

An optimal estimator \mathbf{H}_{GSA} based on the generalized subspace approach (GSA) can then be obtained by applying Eq. (35) and Eq. (36) to Eq. (29):

$$\begin{aligned} \mathbf{H}_{GSA} &= \mathbf{V}^{-T} \mathbf{D} \mathbf{V}^{-1} \left(\mathbf{V}^{-T} \mathbf{D} \mathbf{V}^{-1} + \mu \mathbf{V}^{-T} \mathbf{I} \mathbf{V}^{-1} \right)^{-1} \\ &= \mathbf{V}^{-T} \mathbf{D} (\mathbf{D} + \mu \mathbf{I})^{-1} \mathbf{V}^{+T} \\ &= \mathbf{V}^{-T} \mathbf{G} \mathbf{V}^T \quad \text{where } \mathbf{G} = \mathbf{D} (\mathbf{D} + \mu \mathbf{I})^{-1} \end{aligned} \quad (37)$$

Based on Eq. (19) and Eq. (37), the EP is then estimated as

$$\begin{aligned} \hat{\mathbf{x}} &= \mathbf{H}_{GSA} \cdot \mathbf{y} \\ &= \mathbf{V}^{-T} \mathbf{G} \mathbf{V}^T \cdot \mathbf{y} \quad \text{where } \mathbf{G} = \mathbf{D} (\mathbf{D} + \mu \mathbf{I})^{-1} \end{aligned} \quad (38)$$

At a glance, the structure of Eq. (38) looks similar to the Karhunen Loeve transform (KLT) and inverse Karhunen Loeve transform (IKLT), with Eq. (38) having the extra signal subspace gain matrix \mathbf{G} . However, the KLT and IKLT operation caters only for unitary eigenvectors. The eigenvectors \mathbf{V} produced by the generalized ED process are not unitary; nevertheless, complete decorrelation is still achievable using these non-unitary eigenvectors. In brief, the corrupted VEP signal \mathbf{y} in Eq. (38) is decorrelated by the non-KLT matrix \mathbf{V}^T . Then, the transformed signal is modified by the matrix \mathbf{G} . Next, the modified signal is retransformed back into the original form by the non-IKLT matrix \mathbf{V}^{-T} to obtain the desired signal.

3.1.1 Configuration of critical parameters

In the GSA and other subspace techniques, there are several critical parameters that need to be configured properly to achieve optimized enhancement of the desired signal. Among the most important parameters requiring special attentions are frame length, correlation matrix dimension, and subspace dimension.

Frame length

The frame length is very important because it somehow dictates the dimension of the corresponding correlation matrix. In turn, the matrix size influences the statistical contents and the usefulness of the correlation matrix, which will be used later in the signal and noise separation. The frame length N must be larger than the order of the assumed signal model, or the dimension of the signal subspace. This is to ensure that a reasonable correlation matrix size bearing sufficient statistics can be generated from the given frame length. As a general rule, N should not be too small or too large. If N is too small, then the amount of statistical data in the correlation matrix will be affected; too large a value will be computationally expensive on the ED of the correlation matrix. In general, N is taken to be three to four times the order of the signal model.

Correlation matrix dimension

The correlation matrix dimension is carried out to $0.4m$ (rounded to the nearest integer) for each side of the autocorrelation curve shown in Fig. 1 below, where $-(N-1) \leq m \leq N-1$; N is the frame length and m is the distance or *lag* between data points. The region bounded by $-0.4m$ and $+0.4m$ contains majority of the statistical information about the signal under study. Beyond the shaded region the autocorrelation pairs at the positive and corresponding negative lags diminishes radically, making the calculation unreliable.

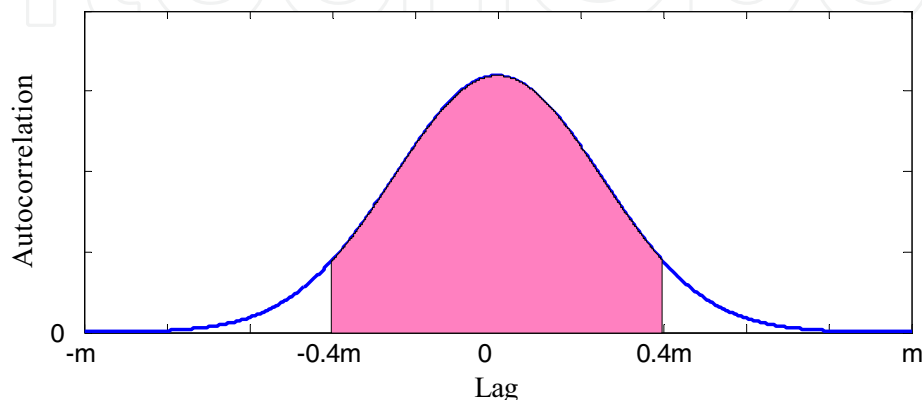


Fig. 1. The shaded area containing reliable statistical information for the correlation (covariance) matrix computation.

Dimension of signal subspace

In general, the dimension (i.e., rank) of the signal subspace is not known *a-priori*. The proper dimension of the signal subspace is critical since too low or too high an estimated dimension yield inaccurate VEP peaks. If the dimension chosen is too low, a highly smoothed spectral estimate of the VEP waveform is produced, affecting the accuracy of the desired peaks. On the other hand, too high a dimension introduces a spurious detail in the estimated VEP waveform, making the discrimination between the desired and unwanted peaks very difficult. It is crucial to note that as the SNR increases, the separation between the signal eigenvalues and the noise eigenvalues increases. In other words, for reasonably high SNRs (≥ 5 dB), the signal subspace dimension can be readily obtained by observing the distinctive gap in the eigenvalue spectrum of the basis matrix covariance. As the SNR reduces, the gap gets less distinctive and the pertinent signal and noise eigenvalues may be significantly larger than zero.

As such, the choice of the dimension solely based on the non-zero eigenvalues as devised by some researchers tends to overestimate the actual dimension of the signal subspace. To overcome the dimension overestimation, some criteria need to be utilized so that the actual signal subspace dimension can be estimated more accurately, preventing information loss or suppressing unwanted details in the recovered signal. There exist many different approaches for information theoretic criteria for model identification purposes. Two well known approaches are Akaike information criteria (AIC) by (Akaike, 1973) and minimum

description length (MDL) by (Schwartz, 1978) and (Rissanen, 1978). In this study, the criteria to be adapted is the AIC approach which has been extended by (Wax & Kailath, 1985) to handle the signal and noise subspace separation problem from the N snapshots of the corrupted signals. For our purpose, we consider only one snapshot ($N = 1$) of the contaminated signal at one particular time. Assuming that the eigenvalues of the observed signal (from one snapshot) are denoted as $\lambda_1 \geq \lambda_2 \geq \dots \geq \lambda_p$, we obtain the following:

$$AIC(k) = 2 \ln \left(\frac{\left[\frac{1}{P-k} \sum_{j=k+1}^P \lambda_j \right]^{P-k}}{\prod_{j=k+1}^P \lambda_j} \right) + 2k(2P-k) \quad (39)$$

The desired signal subspace dimension L is determined as the value of $k \in [0, P-1]$ for which the AIC is minimized.

3.1.2 The implementation of GSA technique

Step 1. Compute the covariance matrix of the brain background colored noise R_n , using the pre-stimulation EEG sample.

Step 2. Compute the noisy VEP covariance matrix R_y , using the post-stimulation EEG sample.

Step 3. Estimate the covariance matrix of the noiseless VEP sample as $R_x = R_y - R_n$.

Step 4. Perform the generalized eigendecomposition on R_x and R_n to satisfy Eq. (34) and obtain the eigenvector matrix V and the eigenvalue matrix D .

Step 5. Estimate the dimension L of the signal subspace using Eq. (39).

Step 6. Form a diagonal matrix D_L , from the largest L diagonal values of D .

Step 7. Form a matrix V_L by retaining only the eigenvectors of V that correspond to the largest L eigenvalues.

Step 8. Choose a proper value for μ as a compromise between signal distortion and noise residues. Experimentally, $\mu = 8$ is found to be ideal.

Step 9. Compute the optimal linear estimator as outlined in Eq. (37).

Step 10. Estimate the clean VEP signal using Eq. (38).

3.2 Subspace Regularization Method

The subspace regularization method (SRM) (Karjalainen et al., 1999) is combining regularization and Bayesian approaches for the extraction of EP signals from the measured data.

In SRM, a model for the EP utilizing a linear combination of some basis vectors as governed by Eq. (18), is used. Next, the linear observation model of Eq. (18) is further written as

$$\mathbf{y} = \mathbf{H}\boldsymbol{\theta} + \mathbf{n} \quad (40)$$

where, $\boldsymbol{\theta} \in \mathfrak{R}^L$ represents an L -dimensional parameter vector that needs to be estimated; $\mathbf{H} \in \mathfrak{R}^{K \times L}$ is defined as the $K \times L$ -dimensional basis matrix that does not contain parameters to be estimated. \mathbf{H} is a predetermined pattern based on certain assumptions to be discussed below. As can be deduced from Eq. (40), the estimated EP signal \mathbf{x} in Eq. (18) is related to \mathbf{H} and $\boldsymbol{\theta}$ in the following way:

$$\mathbf{x} = \mathbf{H}\boldsymbol{\theta} \quad (41)$$

The clean EP signal \mathbf{x} in Eq. (41) is modeled as a linear combination of basis vectors $\boldsymbol{\Psi}_i$ which make up the columns of the matrix $\mathbf{H} = [\boldsymbol{\Psi}_1, \boldsymbol{\Psi}_2, \dots, \boldsymbol{\Psi}_p]$. In general, the generic basis matrix \mathbf{H} may comprise equally spaced Gaussian-shaped functions (Karjalainen et al., 1999) derived from the individual $\boldsymbol{\Psi}_i$, given by the following equation:

$$\boldsymbol{\Psi}_i(t) = e^{-\frac{(t-\tau_i)^2}{2d^2}} \quad \text{for } t = 1, 2, \dots, K \quad (42)$$

where d represents the variance (width) and τ_i represents the mean (position) of the function peak for the given $i = 1, 2, \dots, p$. Once the parameter \mathbf{H} is established and $\boldsymbol{\theta}$ is estimated, the single-trial EP can then be determined as follows:

$$\hat{\mathbf{x}} = \mathbf{H}\hat{\boldsymbol{\theta}} \quad (43)$$

where the hat (^) placed over the \mathbf{x} and $\boldsymbol{\theta}$ symbols indicates the "estimate" of the respective vector.

3.2.1 Regularized least squares solution

The parameter $\boldsymbol{\theta}$ can be approximated by using a generalized Thikonov regularized least squares solution stated as:

$$\hat{\boldsymbol{\theta}}_\alpha = \arg \min_{\boldsymbol{\theta}} \left\{ \|\mathbf{L}_1(\mathbf{y} - \mathbf{H}\boldsymbol{\theta})\|^2 + \alpha^2 \|\mathbf{L}_2(\boldsymbol{\theta} - \boldsymbol{\theta}^*)\|^2 \right\} \quad (44)$$

where \mathbf{L}_1 and \mathbf{L}_2 are the regularization matrices; α is the value of the regularization parameter; $\boldsymbol{\theta}^*$ is the initial (prior) guess for the solution. The solution in Eq. (44) is in fact the most commonly used method of regularization of ill-posed problems; Eq. (44) is a modification of the ordinary weighted least squares solution given as

$$\hat{\theta}_{LS} = \arg \min_{\theta} \left\{ \left\| L_1(\mathbf{y} - \mathbf{H}\theta) \right\|^2 \right\} \quad (45)$$

Furthermore, the regularization parameter α in Eq. (44) controls the weight of the side constraint

$$\left\| L_2(\theta - \theta^*) \right\|^2 \quad (46)$$

so that minimization is achieved. Subsequently, Eq. (44) can be simplified further (Karjalainen et al., 1999) to yield

$$\hat{\theta}_{\alpha} = (\mathbf{H}^T \mathbf{W}_1 \mathbf{H} + \alpha^2 \mathbf{W}_2)^{-1} (\mathbf{H}^T \mathbf{W}_1 \mathbf{y} + \alpha^2 \mathbf{W}_2 \theta^*) \quad (47)$$

where, $\mathbf{W}_1 = L_1^T L_1$ and $\mathbf{W}_2 = L_2^T L_2$ are positive definite weighting matrices.

3.2.2 Bayesian estimation

The regularization process has a close relationship with the Bayesian approach. In addition to the current information of the parameter (e.g. θ) under study, both methods also include the previous parameter information in their computation. In Bayesian estimation, both θ and \mathbf{n} in Eq. (40) are treated as random and uncorrelated with each other. The estimator $\hat{\theta}$ that minimizes the mean square Bayes cost

$$\mathbf{B}_{MS} = E \left\{ \left\| \theta - \hat{\theta} \right\|^2 \right\} \quad (48)$$

is given by the conditional mean

$$\hat{\theta} = E \{ \theta | \mathbf{y} \} \quad (49)$$

of the posterior distribution

$$p(\theta | \mathbf{y}) \propto p(\mathbf{y} | \theta) p(\theta) \quad (50)$$

Subsequently, a linear mean square estimator, known in Bayesian estimation as the maximum a posteriori estimator (MAP) is expressed as

$$\hat{\theta}_{MS} = (\mathbf{H}^T \mathbf{R}_n^{-1} \mathbf{H} + \mathbf{R}_{\theta}^{-1})^{-1} (\mathbf{H}^T \mathbf{R}_n^{-1} \mathbf{y} + \mathbf{R}_{\theta}^{-1} \eta_{\theta}) \quad (51)$$

where, \mathbf{R}_n is the covariance matrix of the EEG noise \mathbf{n} ; \mathbf{R}_{θ} and η_{θ} are the covariance matrix and the mean of the parameter θ , respectively—they represent the initial (prior) information for the parameters θ . Equation (51) minimizes Eq. (48) providing that

- the errors \mathbf{n} are jointly Gaussian with zero mean.
- the parameters θ are jointly Gaussian random variables.

The covariance matrix \mathbf{R}_{θ} can be assumed to be zero if it is not known. In this case, the estimator in Eq. (51) reduces to the ordinary minimum Gauss-Markov estimator given as

$$\hat{\theta}_{GM} = (\mathbf{H}^T \mathbf{R}_n^{-1} \mathbf{H})^{-1} \mathbf{H}^T \mathbf{R}_n^{-1} \mathbf{y} \quad (52)$$

Next, the estimator in Eq. (52) is equal to the ordinary least squares estimator if the noise are independent with equal variances (i.e., $\mathbf{R}_n = \sigma_n^2 \mathbf{I}$); that is

$$\hat{\theta}_{LS} = (\mathbf{H}^T \mathbf{H})^{-1} \mathbf{H}^T \mathbf{y} \quad (53)$$

As a matter of fact, Eq. (53) is the Bayesian interpretation of Eq. (47).

3.2.3 Computation of side constraint regularization matrix

As stated previously, the basis matrix \mathbf{H} could be produced by using sampled Gaussian or sigmoid functions, mimicking EP peaks and valleys. A special case exists if the column vectors that constitute the basis matrix \mathbf{H} are mutually orthonormal (i.e., $\mathbf{H}^T \mathbf{H} = \mathbf{I}$). The least squares solution in Eq. (53) can be simplified as

$$\hat{\theta}_{LS} = \mathbf{H}^T \mathbf{y} \quad (54)$$

For clarity, let \mathbf{J} be a new basis matrix that represents mutually orthonormal basis vectors. Now, the least squares solution in Eq. (54) is modified as

$$\hat{\theta}_{LS} = \mathbf{J}^T \mathbf{y} \quad (55)$$

The regularization matrix L_2 is to be derived from an optimal number of column vectors making up the basis matrix \mathbf{J} . The reduced number of \mathbf{J} columns, representing the optimal set of the \mathbf{J} basis vectors, can be determined by computing the covariance of $\hat{\theta}_{LS}$ in Eq. (55); that is,

$$\begin{aligned} \mathbf{R}_\theta &= E\{\hat{\theta}_{LS} \hat{\theta}_{LS}^T\} = E\{\mathbf{J}^T \mathbf{y} (\mathbf{J}^T \mathbf{y})^T\} \\ &= E\{\mathbf{J}^T \mathbf{y} \mathbf{y}^T \mathbf{J}\} = \mathbf{J}^T \mathbf{R}_y \mathbf{J} \\ &= \text{diag}(\lambda_1, \lambda_2, \dots, \lambda_q) = \Lambda_y \end{aligned} \quad (56)$$

where λ_1 through λ_q represent the diagonal eigenvalues of Λ_y . Equation (56) reveals that the correlation matrix \mathbf{R}_θ is related to the observation vector correlation matrix \mathbf{R}_y . Specifically, \mathbf{R}_θ is equal to the the $q \times q$ -dimensional eigenvalue matrix Λ_y . In other words, \mathbf{R}_θ is the eigenvalue matrix of \mathbf{R}_y , which is the observation vector correlation matrix. Also, the $q \times q$ -dimensional matrix \mathbf{J} is actually the eigenvector matrix of \mathbf{R}_y . Even though there are q diagonal eigenvalues, the reduced basis matrix \mathbf{J} , denoted as \mathbf{J}_x , is the $q \times p$ dimensional eigenvectors that are associated with the p largest (i.e., non-zero) eigenvalues of Λ_y . It is further assumed that \mathbf{J}_x contains an orthonormal basis of the subspace P . It is desirable that the EP $\mathbf{x} = \mathbf{H}\theta$ is closely within this subspace. The projection of \mathbf{x} onto P is denoted as $(\mathbf{J}_x \mathbf{J}_x^T) \mathbf{H}\theta$. The distance between \mathbf{x} and P is

$$\|\mathbf{H}\theta - (\mathbf{J}_x \mathbf{J}_x^T) \mathbf{H}\theta\| = \|(\mathbf{I} - \mathbf{J}_x \mathbf{J}_x^T) \mathbf{H}\theta\| \quad (57)$$

The value of L_2 should be carefully chosen to minimize the side constraint in Eq. (46) which reduces to $\|L\theta\|$ for $\theta^* = 0$. From the inspection of Eq. (57), it can be stated that $L_2 = (I - J_x J_x^T)H$. It is now assumed that L_2 is *idempotent* and *symmetric* such that

$$\begin{aligned} W_2 &= L_2^T L_2 = \left((I - J_x J_x^T)H \right)^T (I - J_x J_x^T)H \\ &= H^T (I - J_x J_x^T)^T (I - J_x J_x^T)H \\ &= H^T (I - J_x J_x^T)H \end{aligned} \quad (58)$$

3.2.4 Combination of regularized solution and Bayesian estimation

A new equation is to be generated based on Eq. (47) and Eq. (51); comparisons between these two equations reveal the following relationships:

- $R_n^{-1} = W_1$, where $W_1 = L_1^T L_1$.
- $R_\theta^{-1} = \alpha^2 W_2$, where $W_2 = L_2^T L_2$.
- $\eta_\theta = \theta^*$.

The weight $W_1 = L_1^T L_1$ can be represented by R_n^{-1} since the covariance of the EEG noise R_n can be estimated from the pre-stimulation period, during which the EP signal is absent. On the contrary, the term R_θ^{-1} is represented by its equivalent $W_2 = L_2^T L_2$ term obtained from Eq. (58). The new solution based on Eq. (47) and Eq. (51) can now be written as

$$\hat{\theta} = \left(H^T R_n^{-1} H + \alpha^2 H^T (I - J_x J_x^T) H \right)^{-1} \left(H^T R_n^{-1} y + \alpha^2 H^T (I - J_x J_x^T) H \theta^* \right) \quad (59)$$

Equation (59) is simplified further by treating the prior value θ^* as zero:

$$\hat{\theta} = \left(H^T R_n^{-1} H + \alpha^2 H^T (I - J_x J_x^T) H \right)^{-1} H^T R_n^{-1} y \quad (60)$$

Therefore, the estimated VEP signal, \hat{x} , from Eq. (43) can be expressed as

$$\begin{aligned} \hat{x} &= H \hat{\theta} \\ &= H \left(H^T R_n^{-1} H + \alpha^2 H^T (I - J_x J_x^T) H \right)^{-1} H^T R_n^{-1} y \end{aligned} \quad (61)$$

3.2.5 Strength of the SRM algorithm

The structure of the algorithm in Eq. (61) resembles that of the Karhunen-Loeve transform, with H^T as the KLT matrix and H as the inverse KLT matrix. Equation (61) does have extra terms (besides H^T and H) which are used for fine tuning. The inclusion of the R_n^{-1} term indicates that a pre-whitening stage is incorporated, and the algorithm is able to deal with both white and colored noise.

3.2.6 Weaknesses of the SRM algorithm

The basis matrix, which serves as one of the algorithm parameters, needs to be carefully formed by selecting a generic function (e.g., Gaussian or sigmoid) and setting its amplitudes and widths to mimic EP characteristics. Simply, the improper selection of such a parameter with a predetermined shape (i.e., amplitudes and variance) somehow pre-meditates or influences the final outcome of the output waveform.

3.3 Subspace Dynamical Estimation Method

The subspace dynamical estimation method (SDEM) has been proposed by (Georgiadis et al., 2007) to extract EPs from the observed signals.

In SDEM, a model for the EP utilizes a linear combination of vectors comprising a brain activity induced by stimulation and other brain activities independent of the stimulus. Mathematically, the generic model for a single-trial EP follows Eq. (18) and Eq. (40), as this work is an extension of that proposed earlier by (Karjalainen et al., 1999).

3.3.1 Bayesian estimation

The SDEM scheme makes use of Eq. (48) through Eq. (53) that lead to Eq. (54). In SDEM, the regularized least squares solution is not included. Also, the basis matrix \mathbf{H} is not produced by using sampled Gaussian or sigmoid functions; the basis matrix will solely be based on the observed signal under study. For clarity, let \mathbf{Z} be a new basis matrix that represents mutually orthonormal basis vectors to be determined. Now, the least squares solution in Eq. (55) is modified as

$$\hat{\boldsymbol{\theta}}_{LS} = \mathbf{Z}^T \mathbf{y} \quad (62)$$

Based on Eq. (56), it can be deduced that \mathbf{Z} in Eq. (62) is actually the eigenvector matrix of \mathbf{R}_y . The \mathbf{Z} term in Eq. (62) can now be represented by its reduced form \mathbf{Z}_x which is associated with the p largest (i.e., non-zero) eigenvalues of Λ_y . It is also assumed that \mathbf{Z}_x contains an orthonormal basis of the subspace P . Equation (62) is therefore written as

$$\hat{\boldsymbol{\theta}} = \mathbf{Z}_x^T \mathbf{y} \quad (63)$$

Therefore, the estimated VEP signal, $\hat{\mathbf{x}}$, from Eq. (43) can be expressed as

$$\hat{\mathbf{x}} = \mathbf{Z}_x \cdot \mathbf{Z}_x^T \cdot \mathbf{y} \quad (64)$$

The structure in Eq. (64) is actually the Karhunen Loeve transform (KLT) and inverse Karhunen Loeve transform (IKLT), since the eigenvectors \mathbf{Z} which is derived from the eigendecomposition of the symmetric matrix \mathbf{R}_y is always unitary. What is achieved in Eq. (64) is that the corrupted EP signal \mathbf{y} is decorrelated by the KLT matrix \mathbf{Z}_x^T . Then, the transformed signal (matrix) is truncated to a certain dimension to suppress the noise segments. Next, the modified signal is retransformed back into the original form by the IKLT matrix \mathbf{Z}_x to obtain the desired signal.

3.3.2 Strength of the SDEM algorithm

The state space model is dependent on a basis matrix to be directly produced by performing eigendecomposition operation on the correlation matrix of the noisy observation. Contrary to SRM, SDEM makes no assumption about the nature of the EP.

3.3.3 Weaknesses of the SDEM algorithm

The SDEM algorithm will work well for any signal that is corrupted by white noise since the eigenvectors of the corrupted signal is assumed to be the eigenvectors of the clean signal and white noise. When the noise becomes colored, the assumption will no longer hold and the algorithm becomes less effective.

4. Results and Discussions

The three subspace techniques discussed above are tested and assessed using artificial and real human data.

The subspace methods under study are applied to estimate visual evoked potentials (VEPs) which are highly corrupted by spontaneous electroencephalogram (EEG) signals. Thorough simulations using realistically generated VEPs and EEGs at SNRs ranging from 0 to -10 dB are performed. Later, the algorithms are assessed in their abilities to detect the latencies of the P100, P200 and P300 components.

Next, the validity and the effectiveness of the algorithms to detect the P100's (used in objective assessment of visual pathways) are evaluated using real patient data collected from a hospital. The efficiencies of the studied techniques are then compared among one another.

4.1 Results from Simulated Data

In the first part of this section, the performances of the GSA, SRM, and SDEM in estimating the P100, P200, and P300 are tested using artificially generated VEP signals corrupted with colored noise at different SNR values.

Artificial VEP and EEG waveforms are generated and added to each other in order to create a noisy VEP. The clean VEP, $x(k) \in \mathcal{R}^M$, is generated by superimposing J Gaussian functions, each of which having a different amplitude (A), variance (σ^2) and mean (μ) as given by the following equations (Andrews et al., 2005).

$$x(k) = \left[\sum_{n=1}^J g_n(k) \right]^T \quad (65)$$

where $g_n(k) = [g_{n1}, g_{n2}, \dots, g_{nM}]$, for $k = 1, 2, \dots, M$, with the individual g_{nk} given as

$$g_{nk} = \frac{A_n}{\sqrt{2\pi\sigma_n^2}} e^{-\frac{(k-\mu_n)^2}{2\sigma_n^2}} \quad (66)$$

The values for A , σ and μ are experimentally tweaked to create arbitrary amplitudes with precise peak latencies at 100 ms, 200 ms, and 300 ms simulating the real P100, P200 and P300, respectively.

The EEG colored noise $e(k)$ can be characterized by an autoregressive (AR) model (Yu et al., 1994) given by the following equation.

$$e(k) = 1.5084e(k-1) - 0.1587e(k-2) - 0.3109e(k-3) - 0.0510e(k-4) + w(k) \quad (67)$$

where $w(k)$ is the input driving noise of the AR filter and $e(k)$ is the filter output. Since noise is assumed to be additive, Eq. (65) and Eq. (67) are combined to obtain

$$y(k) = x(k) + e(k) \quad (68)$$

As a preliminary illustration, Fig. 2 below shows, respectively, a sample of artificially generated VEP, a noisy VEP at SNR = -2 dB, and the extracted VEPs using the GSA, SRM and SDEM techniques.

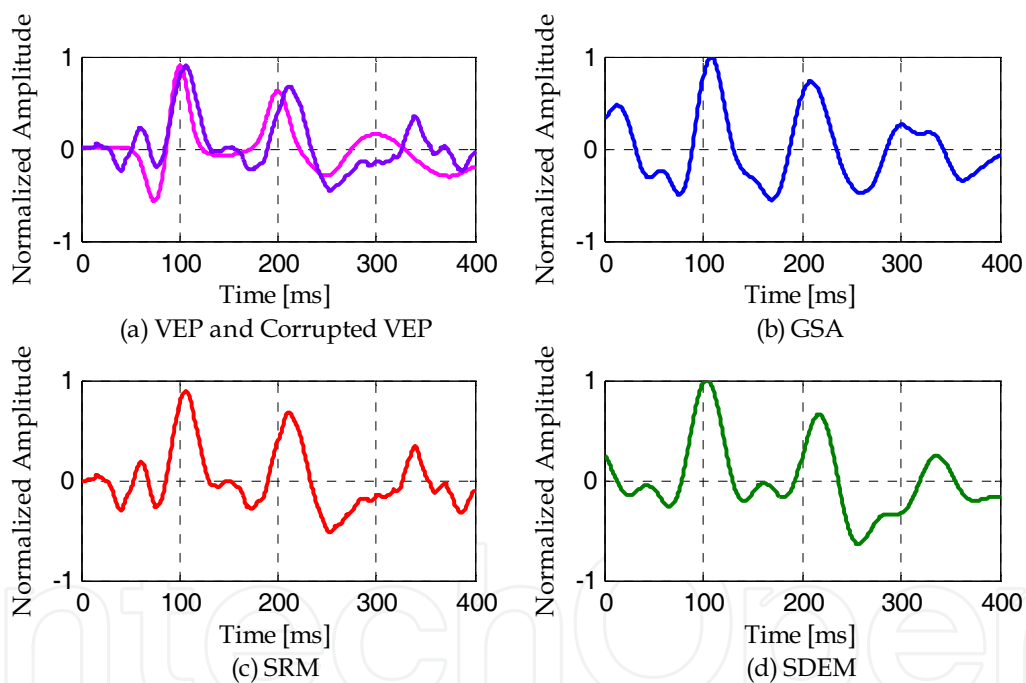


Fig. 2. (a) clean VEP (lighter line/color) and corrupted VEP (darker line/color) with SNR = -2 dB; and the estimated VEPs produced by (b) GSA; (c) SRM; (d) SDEM.

To compare the performances of the algorithms in statistical form, SNR is varied from 0 dB to -13 dB and the algorithms are run 500 times for each value. The average error in estimating the latencies of P100, P200, and P300 are calculated and tabulated along with the failure rate in Table 1 below. Any trial is noted as a failure with respect to a certain peak if the waveform fails to show clearly the pertinent peak.

SNR [dB]	Peak	Failure rate [%]			Peak	Average error		
		GSA	SRM	SDEM		GSA	SRM	SDEM
0	P100	0.6	0.5	1.6	P100	3.7	3.9	4.1
	P200	0.4	2.6	3.2	P200	3.9	4.2	4.3
	P300	17.8	53.2	40.2	P300	6.5	12.9	9.8
-2	P100	2.2	2.0	2.6	P100	4.1	4.1	4.5
	P200	1.4	7.2	9	P200	4.0	5.1	5.3
	P300	17.8	55.4	46	P300	6.3	13.3	10.8
-4	P100	3.2	2.8	6.6	P100	4.2	4.2	5.1
	P200	5.6	12.2	15.2	P200	4.8	5.8	6.3
	P300	21.4	61.4	48.4	P300	6.6	13.8	11.6
-6	P100	5.5	5.7	13.6	P100	4.2	4.5	6.9
	P200	4.8	22	22.8	P200	4.5	7.6	8
	P300	18.2	60	52.2	P300	6.1	14.0	12.7
-8	P100	8.2	9.8	22.2	P100	4.8	5.7	8.4
	P200	8.2	34.8	34.4	P200	4.7	10.0	10.4
	P300	17.4	59.6	52.4	P300	6.3	14.5	13
-10	P100	6	16.4	28.8	P100	4.4	7.1	9.6
	P200	12.8	37	39.4	P200	5.0	10.6	11.3
	P300	18.6	58.4	56.4	P300	6.1	15.2	13.3

Table 1. The failure rate and average errors produced by GSA, SRM and SDEM.

From Table 1, SRM outperforms GSA and SDEM in terms of failure rate for SNRs equal to 0 through -4 dB; however, in terms of average errors, GSA outperforms SRM and SDEM. From -6 dB and below, GSA is a better estimator compared to both SRM and SDEM.

Overall, it is clear that the proposed GSA algorithm outperforms SRM and SDEM in terms of accuracy and success rate. All the three algorithms display their best performance in estimating the latency of the P100 components in comparisons with the other two peaks.

Further, Fig. 3 below illustrates the estimation of VEPs at SNR equal to -10 dB.

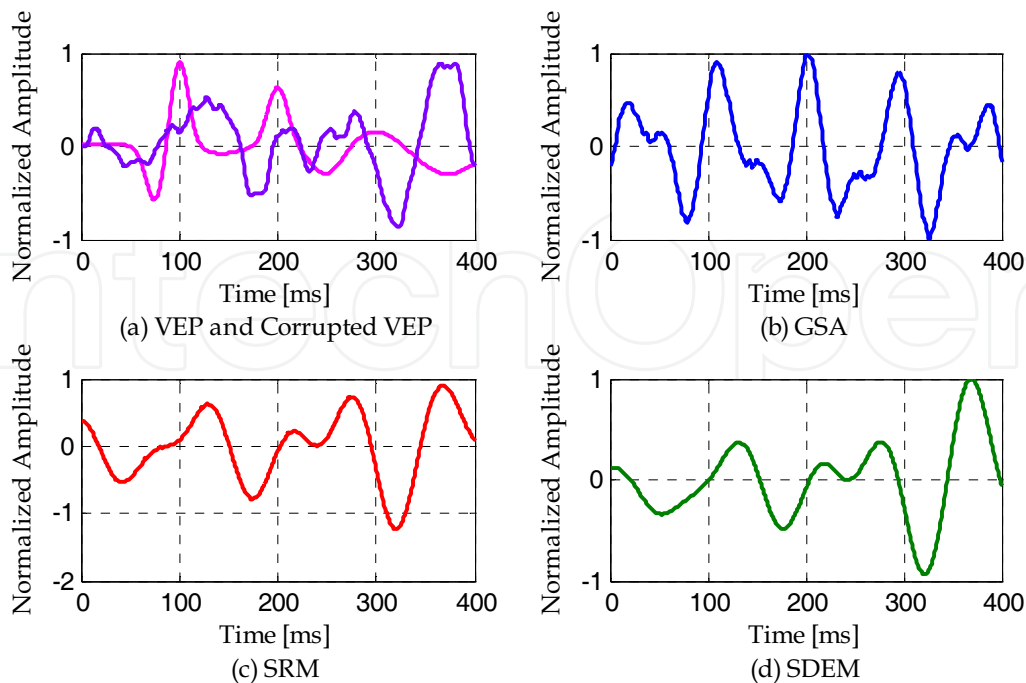


Fig. 3. (a) clean VEP (lighter line/color) and corrupted VEP (darker line/color) with SNR = -10dB; and the estimated VEPs produced by (b) GSA; (c) SRM; (d) SDEM.

4.2 Results of Real Patient Data

This section reveals the accuracy of the GSA, SRM and SDEM techniques in estimating human P100 peaks, which are used by doctors as objective evaluation of the visual pathway conduction. Experiments were conducted at Selayang Hospital, Kuala Lumpur using RETIport32 equipment, and carried out on twenty four subjects having **normal** ($P100 < 115$ ms) and **abnormal** ($P100 > 115$ ms) VEP readings. They were asked to watch a pattern reversal checkerboard pattern (1° full field), the stimulus being a checker reversal ($N = 50$ stimuli). Scalp recordings were made according to the International 10/20 System, with one eye closed at any given time. The active electrode was connected to the middle of the occipital (O1, O2) area while the reference electrode was attached to the middle of the forehead. Each trial was pre-filtered in the range 0.1 Hz to 70 Hz and sampled at 512 Hz.

In this study, we will show the results for artifact-free trials of these subjects taken from their right eyes only. Eighty trials for each subject's right eye were processed by the VEP machine using ensemble averaging (EA). The averaged values were readily available and directly obtained from the equipment. Since EA is a multi-trial scheme, it is expected to produce good estimation of the P100 that can be used as a baseline for comparing the performance of the GSA, SRM and SDEM estimators. Further, GSA and SRM require unprocessed data from the machine. Thus, the equipment was configured accordingly to generate the raw data. The recording for every trial involved capturing the brain activities for 333 ms before stimulation was applied; this enabled us to capture the colored EEG noise alone. The next 333 ms was used to record the post-stimulus EEG, comprising a mixture of the VEP and EEG. The same process was repeated for the consecutive trials.

For comparisons with EA, the eighty different waveforms per subject produced by SSM were also averaged. Again, the strategy here was to look for the highest peak from the averaged waveform. The purpose of averaging the outcome of the SSM was to establish the performance of GSA, SRM and SDEM as single-trial estimators; any mean peak produced by any algorithm will be compared with the EA value. The comparisons shall establish the degree of accuracy of the estimators' individual single-trial outcome.

Illustrated in Fig. 4 below is the estimators' extracted Pattern VEPs for S7 from trial #1.

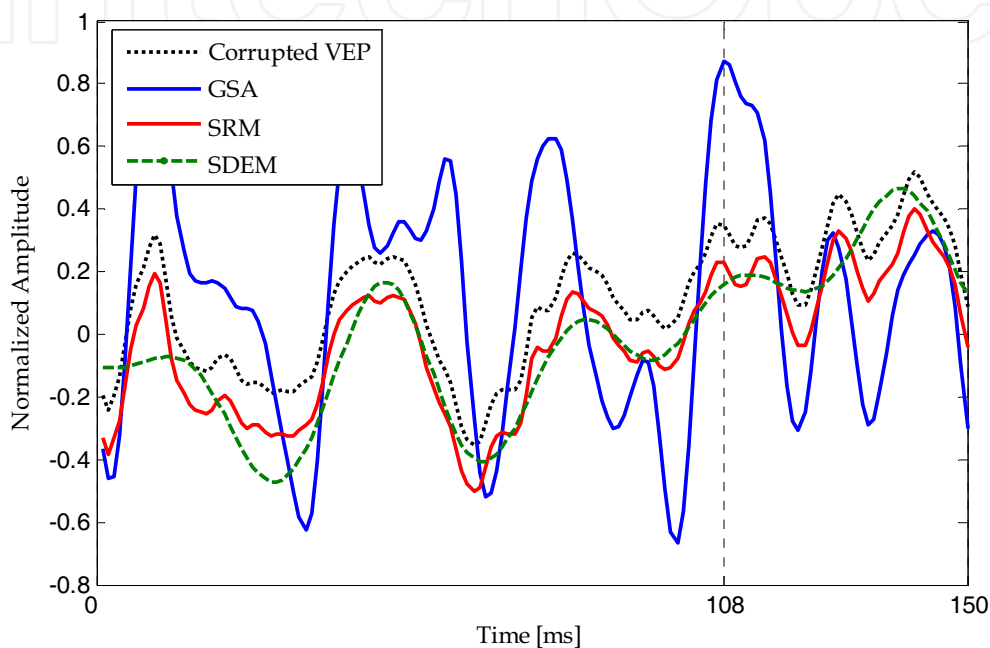


Fig. 4. The P100 of the seventh subject (S7) taken from trial # 1 (note: the P100 produced by the EA method is at 108 ms as indicated by the vertical dotted line).

It is to be noted that any peaks that occur below 90 ms are noise and are therefore ignored. Attention is given to any dominant (i.e., highest) peak(s) from 90 to 150 ms. From Fig. 4, the corrupted VEP (unprocessed raw signal) contains two dominant peaks at 107 and 115 ms, with the one at 115 ms being slightly higher. The highest peak produced by GSA is at 108 ms, which is the same as that obtained by EA. The SRM estimator produces two peaks at 107 and 115 ms, with the most dominant peak at 115 ms. The SDEM algorithm shows the dominant peak at 112 ms. In brief, our GSA technique frequently produces lower mean errors in detecting the P100 components from the real patient data.

Further, Table 2 below summarizes the mean values of the P100's by EA, GSA, SRM and SDEM for the twenty four subjects.

Subject	EA	Latency [ms]			Mean Error		
		GSA	SRM	SDEM	GSA	SRM	SDEM
S1	99	99	101	138	0	2	39
S2	100	100	101	101	0	1	1
S3	119	119	118	117	0	1	2
S4	128	130	125	96	2	3	32
S5	99	118	98	98	19	1	1
S6	107	104	103	103	3	4	4
S7	108	110	110	91	2	2	17
S8	107	103	105	105	4	2	2
S9	130	144	155	155	14	25	25
S10	117	107	106	105	10	11	12
S11	119	115	123	98	4	4	21
S12	114	113	114	116	1	0	2
S13	102	96	100	117	0	2	20
S14	123	118	118	90	5	5	33
S15	102	96	108	117	6	6	15
S16	108	108	107	106	0	1	2
S17	107	107	107	106	0	0	1
S18	107	108	110	111	1	3	4
S19	110	106	104	104	4	6	6
S20	130	130	121	128	0	9	2
S21	109	102	102	101	7	7	8
S22	130	135	148	138	5	13	8
S23	102	104	133	133	2	31	31
S24	102	102	102	102	0	0	0

Table 2. The mean values of the P100's produced by GSA, SRM and SDEM for twenty four subjects.

From Table 2, it is quite clear that GSA outperforms the SRM and SDM techniques in estimating the P100.

5. Conclusion

In this chapter the foundations of the subspace based signal enhancement techniques are outlined. The relationships between the principal subspace (signal subspace) and the maximum energy, and between the complementary subspace (noise subspace) and the minimum energy, are defined. Next, the eigendecomposition of the autocorrelation matrix of data corrupted by additive noise, and how it is used to enhance SNR by retaining only the information in the signal subspace eigenvectors, is explained. Since, finding the dimension of signal subspace is a critical issue to subspace teachings, the Akaike information criteria is suggested to be used. Three subspace based techniques, GSA, SRM and SDEM, exploiting

the concept of signal and noise subspaces in different ways, in order to effectively enhance the SNR in EP environments, are explained. The performances of the techniques are compared using both artificially generated data and real patient data.

In the first experiment, the techniques are used to estimate the latencies of P100, P200, and P300, under SNR varying from 0 dB to -10 dB. The EPs are artificially generated and corrupted by colored noise. The results show better performance by the GSA in terms of both accuracy and failure rate. This is mainly due to the use of the generalized eigendecomposition for simultaneous diagonalization of signal and noise autocorrelation matrices.

In the second experiment the performances are compared using real patient data, and ensemble averaging is used as a baseline. The GSA is showing closer results to the EA, in comparisons with SRM and SDEM. This makes the single-trial GSA technique perform like the multi-trial ensemble averaging in VEP extraction, with the added advantages of recovering the desired peaks of the individual trial, reducing recording time, and relieving subjects from fatigue.

In summary, subspace techniques are powerful if used properly to extract biomedical signals such as EPs which are severely corrupted by additive colored or white noise. Finally, the signal subspace dimension and the Lagrange multiplier are two crucial parameters that influence the estimators' performances, and thus require further studies.

6. Acknowledgment

The authors would like to thank Universiti Teknologi PETRONAS for funding this research project. In addition, the authors would like to thank Dr. Tara Mary George and Mr. Mohd Zawawi Zakaria of the Ophthalmology Department, Selayang Hospital, Kuala Lumpur who acquired the Pattern Visual Evoked Potentials data at the hospital.

7. References

- Akaike, H. (1973). Information Theory and an Extension of the Maximum Likelihood Principle, *Proceedings of the 2nd Int'l. Symp. Inform. Theory, Supp. to Problems of Control and Inform. Theory*, pp. 267-281, 1973.
- Andrews, S.; Palaniappan R. & Kamel N. (2005). Extracting Single Trial Visual Evoked Potentials using Selective Eigen-Rate Principal Components. *World Enformatika Society Transactions on Engineering, Computing and Technology*, vol. 7, August 2005.
- Cui, J.; Wong, W. & Mann, S. (2004). Time-Frequency Analysis of Visual Evoked Potentials by Means of Matching Pursuit with Chirplet Atoms, *Proceedings of the 26th Annual International Conference of the IEEE EMBS*, San Francisco, CA, USA, pp. 267-270, September 1-5, 2004.
- Deprettere, F. (ed.) (1989). *SVD and Signal Processing: Algorithms, Applications and Architectures*, North-Holland Publishing Co., 1989.

- Ephraim, Y. & Van Trees, H. L (1995). A Signal Subspace Approach for Speech Enhancement. *IEEE Transaction on Speech and Audio Processing*, vol. 3, no. 4, pp. 251-266, July 1995.
- Georgiadis, S.D.; Ranta-aho, P. O.; Tarvainen, M. P. & Karjalainen, P. A (2007). A Subspace Method for Dynamical Estimation of Evoked Potentials. *Computational Intelligence and Neuroscience*, vol. 2007, article ID 61916, pp. 1-11, September 18, 2007.
- Gharieb, R. R. & Cichocki, A (2001). Noise Reduction in Brain Evoked Potentials Based on Third-Order Correlations. *IEEE Transactions on Biomedical Engineering*, vol. 48, no. 5, pp. 501-512, May 2001.
- Golub, G. H. & Van Loan, C. F. (1989). *Matrix Computations*, The Johns Hopkins University Press, 2nd edition, 1989.
- Henning, G. & Husar, P. (1995). Statistical Detection of Visually Evoked Potentials. *IEEE Engineering in Medicine and Biology*, July/ August 1995.
- John, E.; Ruchkin, D. & and Villegas, J. (1964). Experimental background: signal analysis and behavioral correlates of evoked potential configurations in cats. *Ann. NY Acad. Sci.*, vol. 112, pp. 362-420, 1964.
- Karjalainen, P. A.; Kaipio, J. P.; Koistinen, A. S. & Vauhkonen, M. (1999). Subspace Regularization Method for the Single-Trial Estimation of Evoked Potentials. *IEEE Transactions on Biomedical Engineering*, vol. 46, no. 7, pp. 849-860, July 1999.
- Nidal-Kamel & Zuki-Yusoff, M. (2008). A Generalized Subspace Approach for Estimating Visual Evoked Potentials, *Proceedings of the 30th Annual Conference of the IEEE Engineering in Medicine and Biology Society (IEEE EMBC'08)*, Vancouver, Canada, Aug. 20-24, 2008, pp. 5208-5211.
- Regan, D. (1989). *Human brain electrophysiology: evoked potentials and evoked magnetic fields in science and medicine*, Elsevier, New York: Elsevier.
- Rissanen, J. (1978). Modeling by shortest data description. *Automatica*, vol. 14, pp. 465-471, 1978.
- Schwartz, G. (1978). Estimating the dimension of a model. *Ann. Stat.*, vol. 6, pp. 461-464, 1978.
- Wax, M. & Kailath, T. (1985). Detection of Signals by Information Theoretic Criteria. *IEEE Transactions on Acoustics, Speech, and Signal Processing*, vol. ASSP-33, no. 2, pp. 387-392, April 1985.
- Yu, X. H.; He, Z. Y. & and Zhang, Y. S (1994). Time-Varying Adaptive Filters for Evoked Potential Estimation. *IEEE Transactions on Biomedical Engineering*, vol. 41, no. 11, November 1994.
- Zuki-Yusoff, M. & Nidal-Kamel (2009). Estimation of Visual Evoked Potentials for Measurement of Optical Pathway Conduction (accepted for publication), *the 17th European Signal Processing Conference (EUSIPCO 2009)*, Glasgow, Scotland, Aug. 24-28, 2009, to be published.
- Zuki-Yusoff, M.; Nidal-Kamel & Fadzil-M.Hani, A. (2008). Single-Trial Extraction of Visual Evoked Potentials from the Brain, *Proceedings of the 16th European Signal Processing Conference (EUSIPCO 2008)*, Lausanne, Switzerland, Aug. 25-29, 2008.
- Zuki-Yusoff, M.; Nidal-Kamel & Fadzil-M.Hani, A. (2007). Estimation of Visual Evoked Potentials using a Signal Subspace Approach, *Proceedings of the International Conference on Intelligent and Advanced Systems 2007 (ICIAS 2007)*, Kuala Lumpur, Malaysia, Nov. 25-28, 2007, pp. 1157-1162.



Biomedical Engineering

Edited by Carlos Alexandre Barros de Mello

ISBN 978-953-307-013-1

Hard cover, 658 pages

Publisher InTech

Published online 01, October, 2009

Published in print edition October, 2009

Biomedical Engineering can be seen as a mix of Medicine, Engineering and Science. In fact, this is a natural connection, as the most complicated engineering masterpiece is the human body. And it is exactly to help our “body machine” that Biomedical Engineering has its niche. This book brings the state-of-the-art of some of the most important current research related to Biomedical Engineering. I am very honored to be editing such a valuable book, which has contributions of a selected group of researchers describing the best of their work. Through its 36 chapters, the reader will have access to works related to ECG, image processing, sensors, artificial intelligence, and several other exciting fields.

How to reference

In order to correctly reference this scholarly work, feel free to copy and paste the following:

Nidal S. Kamel and Mohd Zuki-Yusoff (2009). Subspace Techniques for Brain Signal Enhancement, Biomedical Engineering, Carlos Alexandre Barros de Mello (Ed.), ISBN: 978-953-307-013-1, InTech, Available from: <http://www.intechopen.com/books/biomedical-engineering/subspace-techniques-for-brain-signal-enhancement>

INTECH
open science | open minds

InTech Europe

University Campus STeP Ri
Slavka Krautzeka 83/A
51000 Rijeka, Croatia
Phone: +385 (51) 770 447
Fax: +385 (51) 686 166
www.intechopen.com

InTech China

Unit 405, Office Block, Hotel Equatorial Shanghai
No.65, Yan An Road (West), Shanghai, 200040, China
中国上海市延安西路65号上海国际贵都大饭店办公楼405单元
Phone: +86-21-62489820
Fax: +86-21-62489821

© 2009 The Author(s). Licensee IntechOpen. This chapter is distributed under the terms of the [Creative Commons Attribution-NonCommercial-ShareAlike-3.0 License](https://creativecommons.org/licenses/by-nc-sa/3.0/), which permits use, distribution and reproduction for non-commercial purposes, provided the original is properly cited and derivative works building on this content are distributed under the same license.

IntechOpen

IntechOpen